Int. J. Multiphase Flow Vol. 16, No. 4, pp. 691–712, 1990
Printed in Great Britain.

0301-9322/90 $3.00 + 0.00

FLOW IN SIMULATED POROUS MEDIA

P. M. ADLER,[1] C. G. JACQUIN[2] and J. A. QUIBLIER[2]
[1]Laboratoire d'Aérothermique du CNRS, 4ter route des Gardes, 92190 Meudon, France
[2]Institut Français du Pétrole, B.P. 311, 92506 Rueil-Malmaison, France

(*Received* 15 *June* 1989; *in revised form* 15 *February* 1990)

Abstract—Two average statistical properties of the pore space of Fontainebleau sandstones are measured on thin sections. They are used to generate fictitious porous media which share the same statistical properties as the real ones; the simulation process is thoroughly presented and discussed. The Stokes flow of a Newtonian fluid in such media can be numerically determined by a finite-difference scheme in three dimensions; the permeability of these media is easily derived from these flow fields. The numerical values of permeability are compared to the experimental data. With no adjustable constant, the predicted permeabilities were found to be in acceptable agreement with the experimental ones.

Key Words: porous media, permeability, simulation porosity, correlation

1. INTRODUCTION

The prediction of the permeability of real media is a long-standing problem of very important practical interest. The determination of the permeability is difficult for two main reasons. First, it is usually hard to quantitatively describe the medium in a realistic manner; second, the flow field is a solution of partial differential equations which are not easy to solve except numerically.

Recently, classical methods of numerical analysis were used to obtain the flow fields in any three-dimensional porous medium and were found to yield satisfactory results with reasonable computer times (Lemaître & Adler 1990). On the other hand, an algorithm originally developed in two dimensions (Joshi 1974) was extended to three dimensions (Quiblier 1984); this algorithm can generate porous media with given statistical properties. Finally, the permeability of Fontainebleau sandstones was systematically measured by Jacquin (1964); this geological material is well-known for its homogeneity; thin sections were also made.

Hence all the necessary ingredients for the generation of simulated porous media with imposed properties, the numerical determination of their permeability and the comparison with the experimental permeabilities measured on the same samples were ready to use and could be combined one with the other one.

It is the purpose of the present paper to give an account of this attempt. To the best of our knowledge, we are not aware of such a previous work. The previous simulations reported by Joshi (1974) and Quiblier (1984) were not used in this purpose. Moreover, previous attempts to determine the permeability of porous media were limited to various models which are described and summarized in Adler (1989).

This paper is organized as follows. Section 2 is a brief account of the experimental measurements. The major properties of the Fontainebleau sandstones are recalled first. The measurement of the permeability and the preparation of the thin sections is then discussed at length; two quantities are determined from the pore space: the familiar porosity and the less common autocorrelation function of the pore space.

Sections 3 and 4 are devoted to the simulation of real media. It is shown in section 3 how one can generate a three-dimensional random porous medium with a given porosity and a given correlation function. The medium is made of elementary cubes which are filled by solid or liquid. It can be generated in two steps starting from Gaussian and independent variables $X(\mathbf{x})$. Linear combinations of these variables yield a population $Y(\mathbf{x})$ which is still Gaussian but correlated; the correlation depends upon the set of coefficients a of the linear combinations. This population is then transformed into a discrete population $Z(\mathbf{x})$ which takes only two values, 0 and 1; this transformation can be viewed as a nonlinear function or filter. The correlation of the population

$Y(\mathbf{x})$ is of course modified by this additional filtering; the average value of $Z(\mathbf{x})$ is automatically equal to ε.

The practical simulation of given porous media is addressed in section 4. First one has to solve a sort of inverse problem; this is performed, as previously, in two steps. Since the experimental correlation is known, one has to determine the correlation function of the population $Y(\mathbf{x})$; the possibility of this determination is illustrated and discussed. Then the coefficients a can be calculated; since the present paper is restricted to isotropic media, the determination of these coefficients can be greatly shortened. Some sets of coefficients are given together with the relative precision.

Once these coefficients are known for a given sample, artificial porous media can be generated at will. It is first verified that the statistical properties of the simulated media are close to those of the real media they are supposed to match. The influence of various "artificial" parameters is examined such as the step with which the experimental correlation is sampled. Simulated cross-sections of the simulated media are compared to the thin sections; the visual aspect of the former is quite satisfactory. Thus, it is concluded that the simulation scheme devised by Joshi (1974) and Quiblier (1984) works well.

The calculation of the flow field and of the permeability of these simulated porous media is done in the last section. The fluid problem, the method of solution and the possibilities of the numerical program are first presented briefly. Then the influence of the three "artificial" geometric parameters on the permeability is carefully analysed. A compromise between various constraints is proposed; for a certain choice of values, these parameters do not seem to bias the results too much. The large amplitudes of the statistical fluctuations which are encountered during the Monte Carlo simulation of samples are insisted upon; the obtention of precise statistical averages is hindered by the length of the computations.

The permeabilities corresponding to five porosities are computed and compared with the experimental data. It should be emphasized that there is no fitted constant and that every quantity is measured or calculated. The experimental permeability is at most five times larger than the calculated one; the shape of the experimental curve is predicted quite accurately, as if a systematic "error" has been incorporated in the length scale. The Carman equation is not well verified and the Kozeny constant is much larger than its usual empirical value of 5.

This discrepancy was frustrating though it is, to the best of our knowledge, the first time that such an agreement has been obtained with geological porous media.

Finally, the possible reasons for this relative disagreement are analysed. Among the most promising developments of the present research is the inclusion of additional statistical properties in the simulation.

2. EXPERIMENTAL

We shall insist upon the geometrical properties of the Fontainebleau sandstones and their measurements. The permeability data, which are of a more classical character, will be only briefly recalled.

Materials

Fontainebleau sandstones were selected here because they are known to have remarkable properties for geological materials (Jacquin 1964). They are made of a single mineral, quartz; they do not contain any clay, hence there is no physicochemical interaction between the solid phase and aqueous fluids; permeabilities measured with air and water are usually identical. The geometric structure of these sandstones is quite simple since they display only an intergranular porosity; there is no microporosity inside the particles.

Moreover, they are known to be remarkably homogeneous; another important advantage is the fact that porosity may be varied while, globally, the same structure is conserved.

For all these reasons, many measurements were performed on these sandstones.

Several thin sections of these sandstones are shown in figures 1(a–d). The pore space was obtained by injecting a dyed glue into the medium; then the sample was cut and the pore space replaced by the dye-hardened glue (Zinszner & Meynot 1982). Sections (about 20 μm thick) were

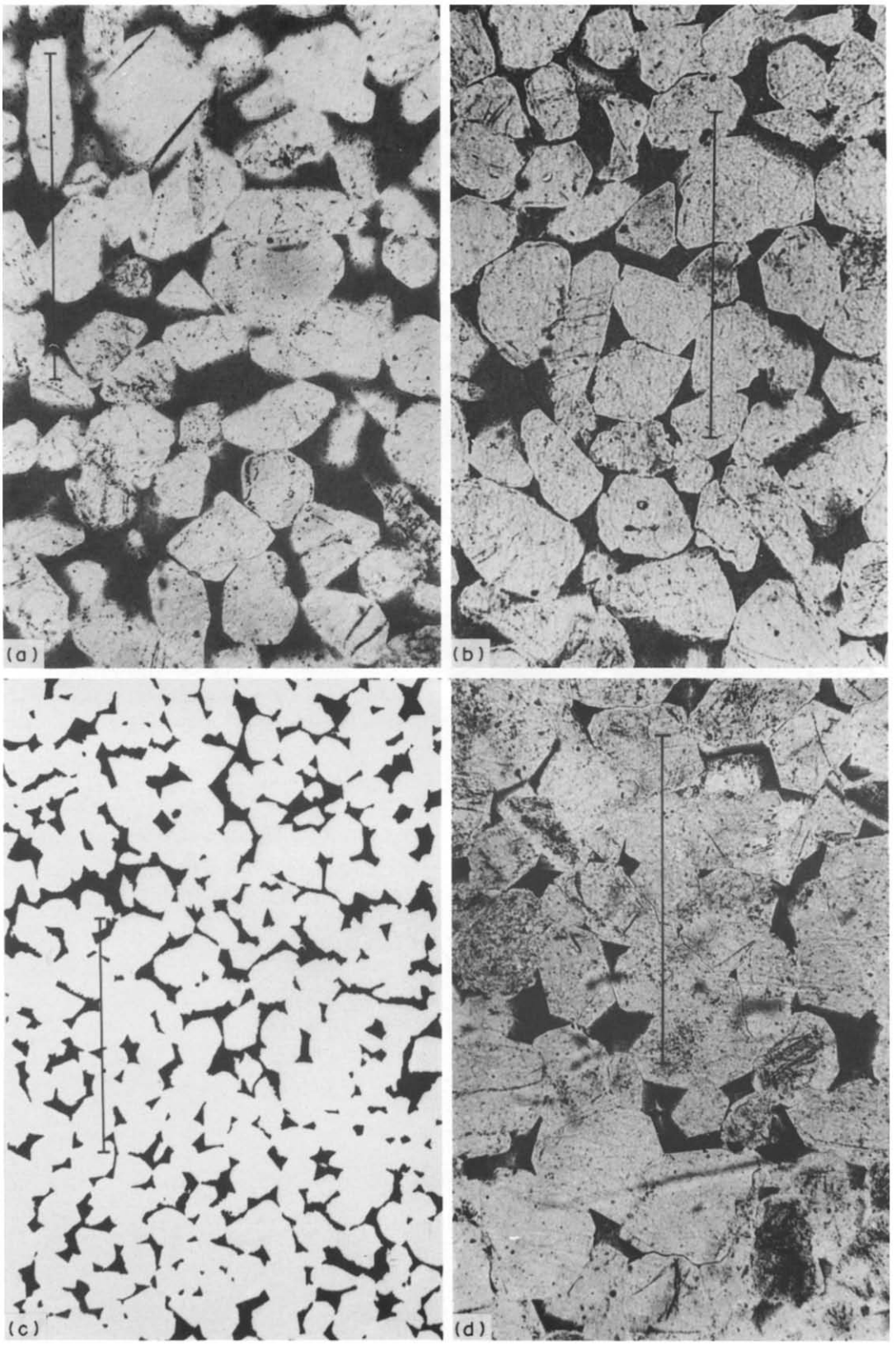

Figure 1. Thin sections of Fontainebleau sandstone. The pore space appears in black. (a), (b) and (d) are real pictures of thin sections, while in (c) the contrast between the solid and the "liquid" phases has been enhanced by various treatments, mostly manual. The scale is indicated on each picture by a bar which corresponds to 0.5 mm. The names and the measured porosity of each picture are as follows: (a) 2A3, $\varepsilon = 0.31$; (b) GF2, $\varepsilon = 0.25$; (c) CJ, $\varepsilon = 0.21$; (d) 12A13, $\varepsilon = 0.11$.

obtained by abrasion of the samples. The pore space is clearly defined since the glue was dyed in red; colour pictures of these sections can be taken with the help of a microscope.

The examples shown in figures 1(a–d) make obvious the fact that this material was originally nonconsolidated sand. Then various geological processes such as the accretion of the sand particles took place with the effect that the porosity decreased. Usually in such sandstones, porosity ranges from 0.03 to 0.35, roughly speaking.

The porosity ε and the permeability K were measured on a large number of cylindrical samples of dia 2.5 cm and length 3–4 cm. The global porosity was measured by comparison of three different weights: weight of the dry sample; weight of the sample saturated with water; and apparent weight of the saturated sample immersed in water. Permeability was measured with air and water on a few samples; except for the small permeabilities where the Klinkenberg effect takes place (Jacquin 1964), no significant difference was observed. Hence all the other measurements were performed with air only.

The permeability data are shown in figure 2. They are taken from Jacquin (1964). It is tempting to correlate them by a power law:

$$K \propto \varepsilon^n, \qquad [1]$$

n was found to be equal to 4.15. This law is in good agreement with the data for the intermediate porosities, but it tends to overestimate K for low and high porosities. It was later proposed by Bourbie *et al.* (1986) to consider two regions; for porosities smaller $<5\%$, n is of the order of 7, while it is equal to 3 when ε ranges from 8 to 25%.

Though important for itself, the comparison of the data with [1] is not crucial here since we are going to compare the numerical predictions with the data themselves.

In this respect, it is interesting to notice the existence of large fluctuations in the data: for the same value of the porosity, the permeability may differ by almost a factor 10. This is not contradictory with our statement about the homogeneous character of the Fontainebleau sandstones; it was shown by Henriette *et al.* (1989) that the permeabilities of limestones may vary by two orders of magnitude.

Image analysis

The porosity and the correlation function of the pore space were measured on each picture.

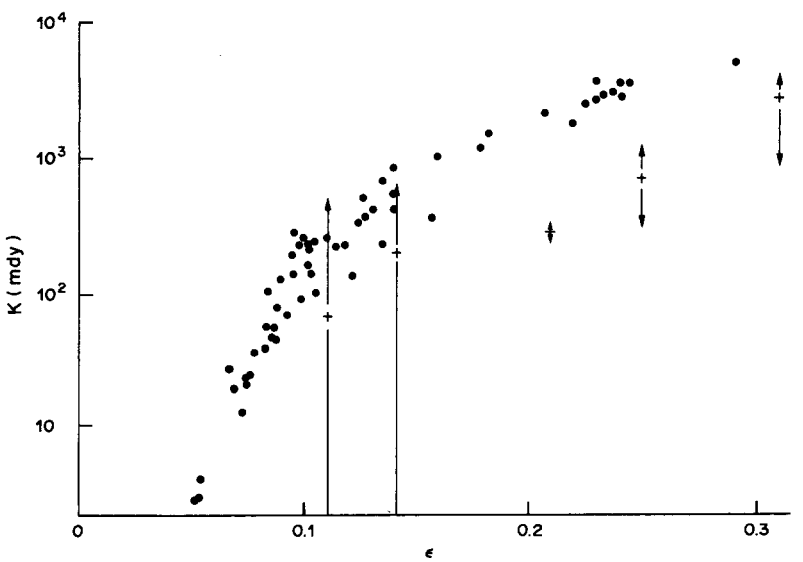

Figure 2. Permeability (for air in mD) as a function of the porosity ε (Jacquin 1964). The dots are the experimental data. The average numerical permeability $\bar{K}$ was calculated for the four previous samples plus an additional one; they are indicated by crosses; data are for $N_c = 27$, $L_c = 8$ and $n = 4$; the vertical bars ↕ indicate the interval of variation of the individual permeabilities.

Let us start with general definitions of these quantities. A phase function $Z(\mathbf{x})$ can be introduced,

$$Z(\mathbf{x}) = \begin{cases} 1 & \text{if } \mathbf{x} \text{ belongs to the pore space,} \\ 0 & \text{otherwise,} \end{cases} \quad [2]$$

where $\mathbf{x}$ denotes the position with respect to an arbitrary origin.

The porosity ε and the correlation function $R_z(\mathbf{u})$ can be defined by the statistical averages (which will be denoted by an overbar):

$$\varepsilon = \bar{Z}(\mathbf{x}) \quad [3a]$$

$$R_z(\mathbf{u}) = \frac{\overline{[Z(\mathbf{x}) - \varepsilon] \cdot [Z(\mathbf{x}+\mathbf{u}) - \varepsilon]}}{(\varepsilon - \varepsilon^2)}, \quad [3b]$$

ε is obviously a positive quantity which is limited to the [0, 1]-interval. A stronger general statement can be made on $R_z(\mathbf{u})$; it can be shown that a function $R_z(\mathbf{u})$ is a correlation function iff all its Fourier components are nonnegative; a more rigorous version of this property can be found in Adler (1981).

It is also interesting to point out that the correlation function of the solid phase is the same as [3b].

When the material is supposed to be homogeneous, the statistical averages can be replaced by volume averages. When it is supposed to be isotropic, these volume averages can be replaced by surface averages; hence the use of thin sections is justified. The surface integrations which correspond to [3a, b] can be easily performed by any software of image analysis.

After these general considerations, let us give some details about the image analysis itself. The first serious difficulty is the transformation of the initial picture [such as figures 1(a, b, d)] into an image which can be readily binarized, such as figure 1(c). Of course, the alteration of the initial image during this step should be minimized. Since our hardware is not sensitive to the colour but only to the grey level, we did not find any other way than to do it manually. The pore space was simply copied on a transparency; when the image has the dimensions of a standard sheet of paper, the precision is good enough.

The subsequent treatment of such black-and-white images is standard. The image is registered and binarized; thanks to the contrast which was manually introduced, a threshold is chosen without any difficulty. The length scale was carefully measured; the length corresponding to 1 pixel will be denoted α (in μm).

The binarized image S is divided into two halves S_1 and S_2. Hence,

$$S = S_1 \cup S_2, \quad S_1 \cap S_2 = \varnothing. \quad [4]$$

The porosity is simply defined as the proportion of pore space contained in a given surface. In order to get an idea of the homogeneity of the sample, this ratio was measured twice, i.e. on S and on S_1. The corresponding values are denoted by ε and ε_1. They are given in figures 3(a–d) for some of the samples which were studied; in these samples, the differences are seen to be quite small; this was not always the case and the constant character of the porosity was one of the criteria to select or not select a thin section.

In order to calculate $R_z(u)$, S_1 is first translated by a distance u along the x-axis; it yields $S_1(+u)$. The spatial average indicated in [3b] is replaced by an intersection of images,

$$\overline{Z(x, y) \cdot Z(x+u, y)} = S_1(+u) \cap S.$$

The other operations indicated in [3b] are then performed algebraically.

The results relative to the images shown in figures 1(a–d) are displayed in figures 3(a–d). Note that the image CJ contains about four times more information than the other three because of the change of scale. The major difference between these images is that (a), (b) and (d) display quite important correlations for large values of u which are almost absent from image (c).

This was thought to be caused by a relative lack of statistics; in order to check this point, the image CJ was divided into four equal parts and the correlation function was measured on each part. The results are displayed in figures 4(a–d). Clearly, the long-range correlations are relatively enhanced when the images are smaller, i.e. when they contain less information; these correlations

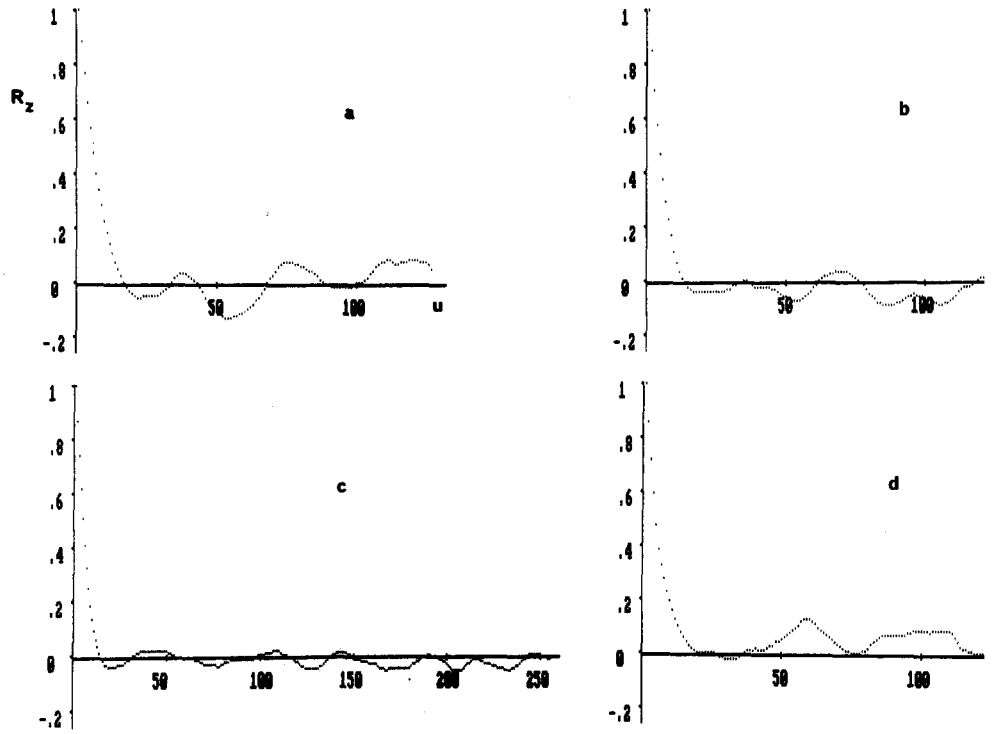

Figure 3. Experimental correlation functions R_z as functions of the translation u. The abscissae are graduated in pixels; the scales are: (a), (b) and (d), $\alpha = 3.8\,\mu$m/pixel; (c) $\alpha = 4.6\,\mu$m/pixel. Images (a), (b) and (d) were analysed with 256 × 256 pixels, while image (c) was analysed with 512 × 512 pixels. These measurements were, of course, performed on the images displayed in figures 1(a–d). The porosities ε and ε_1 are: (a) 0.31, 0.32; (b) 0.24, 0.26; (c) 0.20, 0.21; (d) 0.11, 0.10.

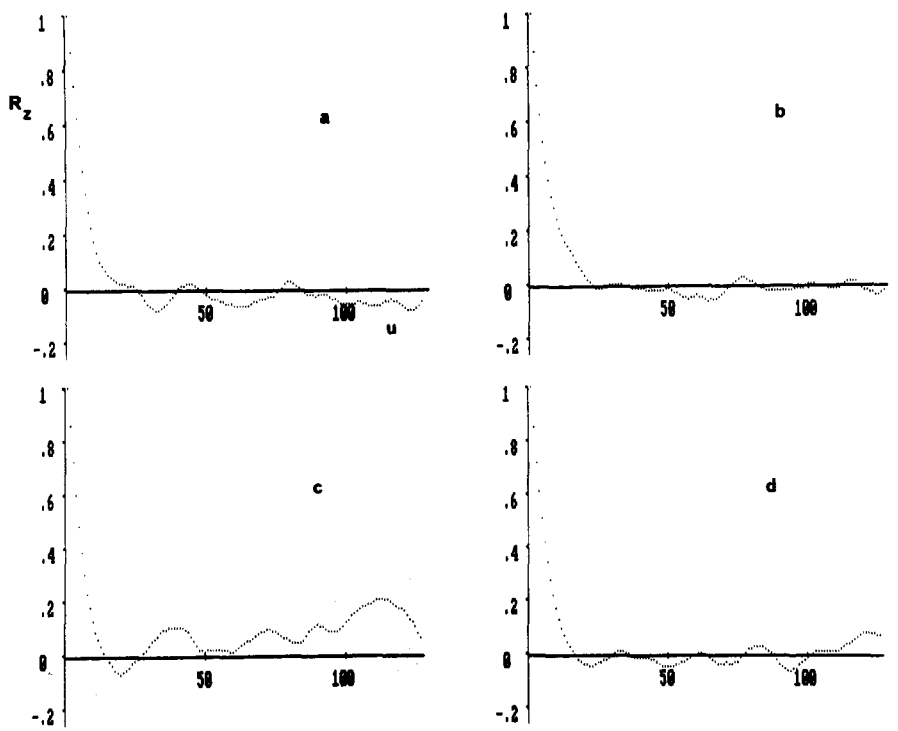

Figure 4. Experimental correlation functions R_z as functions of the translation u. (a)–(d) correspond to one-fourth of the image CJ displayed in figure 1(c). The scale α is always equal to 4.5 μm/pixel. The porosities ε and ε_1 are: (a) 0.21, 0.22; (b) 0.16, 0.15; (c) 0.20, 0.16; (d) 0.14, 0.14. These images were analysed with 256 × 256 pixels.

are different in each image; however it should be noticed that the four correlation functions are very close for short distances u, i.e. when $R_z > 0.2$.

The relative role of the short- and long-range correlation functions on the simulated porous media and on their permeability will be detailed later.

The four correlations displayed in figures 3(a–d) can now be compared one to the other when the same length scale is used (cf. figure 5). Obviously, there is no dramatic change from one sample to another; two of them are largely superimposed while the correlation for the image 12A13 is intermediate between the two former ones and the fourth one. Of course, other representations of these data were tried; for instance a correlation length $\mathfrak{L}$ may be introduced by the formula

$$R_z(u) = e^{-u/\mathfrak{L}}. \qquad [5]$$

Such an expression is well-verified for short distances u only for the image 12A13, i.e. for the lowest porosity; in the other cases the correlation decreases too rapidly. Of course, such an expression is not expected to apply for large u.

No further systematic work was done on this particular point. The concept of a correlation length $\mathfrak{L}$ will be used in section 5 in the loose sense of a length above which the correlation is negligible.

Another check on the quality of the data was done as follows. Since the Fourier coefficients of a correlation function should be positive (Adler 1981), they were systematically calculated for the experimental correlations. Then the negative Fourier coefficients were examined and generally found to be small with respect to the largest positive ones; finally, the correlation functions were reconstructed with the negative coefficients set to zero. The difference from the original functions was negligible since only the third digit was modified, which is of course much smaller than the other experimental errors.

It might be the right point here to try to make some practical recommendations on the measurement of the correlation functions. *A priori* one has to find a compromise between homogeneity and good statistics; the former requirement is easier to fulfil with small images, while the latter one requires large images. The key property now seems to be the statistical homogeneity of the images, a parameter which is roughly estimated by the porosity variations in a given image. This appears to be more important than the extinction of the correlation at long distances since one will not take these distances into account later anyway; it also seems more important than the precision of the short-range correlation since it is not modified very much from one image to the other one.

A good illustration of these considerations is provided by the image CJ displayed in figure 1(c). The long-range correlations is negligible, but it can be seen from figures 4(a–d) that porosity

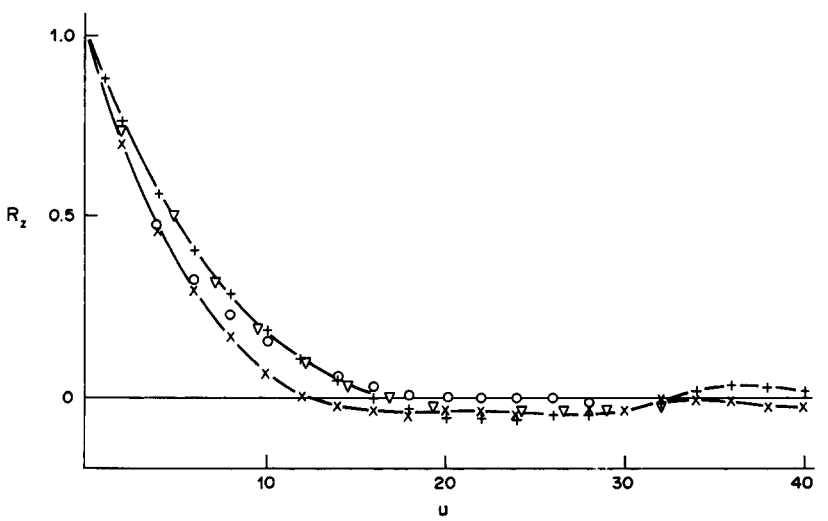

Figure 5. Experimental correlation functions R_z as functions of the translation u. The length scale α is always equal to $\alpha = 3.8\,\mu$m/pixel. Data are for: image 2A3 (+); image GF2 (×); image CJ (▽); image 12A13 (○).

undergoes important variations within the sample. The penalty for good statistics is a relative lack of homogeneity.

3. GENERATION OF RANDOM DISCRETE VARIABLES

Let us first state the purpose of this and the next two sections. We want to generate a three-dimensional random porous medium with a given porosity ε and a given correlation function; the medium is homogenous and—but this last property is not essential—isotropic.

Equivalently, we want to generate a random function of space $Z(\mathbf{x})$ which is equal to 0 in the solid phase and to 1 in the liquid phase. $Z(\mathbf{x})$ has to verify the two average properties (Quiblier 1984). One should emphasize that the point of view is quite different here; ε is a given positive number <1; $R_z(u)$ is a given function of $\mathbf{u}$ which verifies the general properties of a correlation (cf. Adler 1981) but is otherwise arbitrary.

For practical purposes only, the porous medium is constructed in a discrete manner. It is considered as being composed of N_c^3 small cubes, each of the same size a. These elementary cubes are filled either with liquid, or with solid. Examples of such porous media have already been provided elsewhere (Lemaître & Adler 1990; Adler 1989). Hence the spatial variables $\mathbf{x}$ and $\mathbf{u}$ will only take discrete values; the corresponding trios of integers are denoted by

$$\mathbf{x}' = \mathbf{x}/a = (i, j, k) \qquad [6a]$$

and

$$\mathbf{u}' = \mathbf{u}/a = (r, s, t). \qquad [6b]$$

It should be emphasized that the correlation function of isotropic media only depends on the norm of the vector $\mathbf{u}$ (cf. Adler 1981).

An additional condition is imposed by the fact that the sample of generated porous medium has a finite size $a \cdot N_c$. In such a case, it is standard to consider periodic boundary conditions on the sample for the determination of permeability (cf. Adler 1989). The same requirement should be imposed on the generation of the medium itself. Hence, the random field $Z(\mathbf{x})$ has to verify

$$\varepsilon = \bar{Z}(\mathbf{x}) \qquad [7a]$$

and

$$R_z(\mathbf{u}) = \frac{\overline{[Z(\mathbf{x}) - \varepsilon] \cdot [Z(\mathbf{x}_t) - \varepsilon]}}{(\varepsilon - \varepsilon^2)}, \qquad [7b]$$

where the translated vector $\mathbf{x}_t$ is defined as mod $a \cdot N_c$ for each of its components:

$$\mathbf{x}_t = \mathbf{x} + \mathbf{u} \qquad (\text{mod } a \cdot N_c). \qquad [8a]$$

This equality means that, for instance,

$$i_t = i + r \qquad (\text{mod } N_c). \qquad [8b]$$

Thanks to this spatial periodicity, all the physical quantities are independent of the choice of the origin and of the faces of the unit cells.

Several methods certainly exist to generate discrete random variables which verify [7a, b]. Here we shall specialize to isotropic media an algorithm, due to Quiblier (1984), for general three-dimensional porous media. This algorithm was itself an extension of the two-dimensional scheme devised by Joshi (1974).

For sake of clarity, we shall briefly present this algorithm in the present section and recall the major properties of the corresponding random functions. It can be shown that a random and discrete field $Z(\mathbf{x})$ can be devised from a Gaussian field $X(\mathbf{x})$ when the latter one is successively passed through a linear and a nonlinear filter. Let us summarize the influence of these filters and relate their properties to the statistical properties of the resulting fields.

Linear filter

Consider first the initial random field $X(i,j,k)$; the random variables $X(i,j,k)$ are assumed to be normally distributed with a mean equal to 0 and a variance equal to 1; these variables are independent.

A linear operator can be defined by an array of coefficients $a(\mathbf{u}')$, where $\mathbf{u}'$ belongs to a finite cube $[0, L_c]^3$ in Z^3. Outside this cube, it is equal to 0. A new random field $Y(\mathbf{x})$ can be expressed as a linear combination of the random variables $X(\mathbf{x}')$:

$$Y(\mathbf{x}) = \sum_{\mathbf{u}' \in [0, L_c]^3} a(\mathbf{u}')\, X(\mathbf{x}'_t), \qquad [9]$$

where the translated vector $\mathbf{x}'_t$ is defined as mod N_c for each of its components.

The definition [8] is identical to the definition used by Joshi (1974) and Quiblier (1984), except for the periodic character introduced by the condition mod N_c.

This additional condition is imposed by the flow problem which will be solved in section 5; periodic boundary conditions will be imposed on the sample N_c^3.

In order to better understand the necessity of this requirement, one can add a word to describe the result without the condition mod N_c. Suppose that $N_c > L_c$, as will generally be the case. Then the upstream and downstream faces of the sample are statistically independent; this implies that the calculations on the flow field which are implicitly done on an infinite periodic medium whose unit cell is the sample could be completely biased because of this statistical independence; the pores in the upstream and downstream faces being statistically independent have no reason to be connected.

Without any further requirements on the coefficients $a(\mathbf{u}')$ of the linear filter, it can be shown that the random variables $Y(\mathbf{x})$ are Gaussian and centred if $N_c > L_c$.

Let us further assume that the variance of $Y(\mathbf{x})$ is equal to 1,

$$E\{Y^2(\mathbf{x})\} = 1. \qquad [10]$$

Hence the random variables $Y(\mathbf{x})$ have a standard normal distribution, though they are not statistically independent anymore. Their correlation function $R_y(u)$ is easily seen to be

$$R_y(u) = \sum_{r,s,t \in [0, L_c]} a_{r,s,t}\, a_{u+r,s,t}, \qquad [11]$$

where $u + r$ is determined mod N_c.

Nonlinear filter

The random field $Y(\mathbf{x})$ is correlated, but is still not satisfactory since it takes its values in $\mathbb{R}$, while the porous medium has to be represented by a discrete-valued field $Z(\mathbf{x})$ (cf. Joshi 1974).

In order to extract such a field from $Y(\mathbf{x})$, one applies a nonlinear filter G, i.e. the random variable Z is a deterministic function of Y,

$$Z = G(Y). \qquad [12]$$

When G is known, the statistical properties of the random field Z can be derived from those of Y. For the sake of completeness, this derivation, which can be found in Joshi (1974), is briefly repeated here.

Since the random variable $Y(\mathbf{x})$ has a standard normal distribution (i.e. with a zero mean and a variance equal to 1), its distribution function $P(y)$ is given by

$$P(y) = \frac{1}{\sqrt{2\pi}} \cdot \int_{-\infty}^{y} e^{-y/2} \cdot dy. \qquad [13]$$

The deterministic function G is defined by the following condition. When the random variable Y is equal to y, Z takes the value z:

$$z = 1 \quad \text{when } P(y) \leqslant \varepsilon, \qquad [14a]$$

$$z = 0 \quad \text{otherwise.} \qquad [14b]$$

It is, thus, pretty obvious that the average value of $Z(x)$ is equal to ε, and its variance to $\varepsilon - \varepsilon^2$.

The most difficult point consists of the determination of the correlation function $R_z(u)$ of $Z(x)$ as a function of $R_y(u)$. One can start from the fact that the random variable $(Y(\mathbf{x}), Y(\mathbf{x}+\mathbf{u}))$ is a bivariate Gaussian whose probability density is known [cf. Adler (1981), for instance]; this density can be expanded in terms of Hermite polynomials. After some tedious manipulations which use classical identities (Gradshteyn & Ryshik 1965), $R_z(u)$ can be expressed as a series in terms of $R_y(u)$:

$$R_z(u) = \sum_{m=0}^{\infty} C_m^2 \cdot R_y^m(u), \qquad [15]$$

where the coefficients C_m are given by

$$C_m = \frac{1}{\sqrt{2\pi \cdot m!}} \cdot \int_{-\infty}^{+\infty} c(y) \exp\left(-\frac{y^2}{2}\right) H_m(y) \cdot dy, \qquad [16a]$$

together with

$$c(y) = \frac{\varepsilon - 1}{\sqrt{\varepsilon(1-\varepsilon)}} \qquad \text{if } P(y) \leqslant \varepsilon \qquad [16b]$$

and

$$c(y) = \frac{\varepsilon}{\sqrt{\varepsilon(1-\varepsilon)}} \qquad \text{if } P(y) > \varepsilon. \qquad [16c]$$

It should be noticed that the definition of the Hermite polynomials is not standard; the convention used by Joshi (1974) and Quiblier (1984) was adopted here; $H_m(y)$ is defined as

$$H_m(y) = (-1)^m \exp\left(\frac{y^2}{2}\right) \frac{d^m}{dy^m} \exp\left(-\frac{y^2}{2}\right). \qquad [17]$$

The subsequent use of these polynomials in Joshi (1974) and Quiblier (1984) was found to be consistent with this definition.

Finally, the set of the formulae equivalent to [16a–c] is apparently different in Quiblier (1984) due to a typographical mistake.

4. SIMULATION OF A REAL POROUS MEDIA

When one wants to simulate a given porous medium, the first problem is the determination of the correlation function $R_y(u)$ and of the set of coefficients $\bar{a}$: this is what we shall call the inverse problem. Once these coefficients are calculated, porous media can be simulated and their general properties can be critically examined.

In this section, the inverse problem will be addressed first. Then practical applications of the method will be presented and discussed.

The inverse problem

Let us first look at the properties of the nonlinear filter given by the formulae [15]–[17]. It is obvious that

$$R_z(R_y, \varepsilon) = R_z(R_y, 1-\varepsilon). \qquad [18]$$

The limiting case $\varepsilon = 0.5$ is interesting since it can be analytically calculated. By standard manipulations, it may be shown that

$$R_z = \frac{2}{\pi} \cdot \arcsin(R_y), \qquad \varepsilon = \tfrac{1}{2}, \qquad [19]$$

since the coefficients C_m^2 are given by

$$C_1^2 = \frac{2}{\pi}, \qquad [20a]$$

$$C_m^2 = 0 \quad m \text{ even} \qquad [20b]$$

and

$$C_m^2 = \frac{2}{\pi m} \cdot \frac{(m-2)!!}{(m-1)!!} \quad m \geqslant 3, \quad m \text{ odd}. \qquad [20c]$$

The function $R_z(R_y, \varepsilon)$ is represented in figure 6. It was numerically determined as follows. The integral in [16a] was evaluated from y ranging from -10 to $+10$ as in Quiblier (1984); larger integration domains were tried but without any influence on the final result.

The series in [15] is limited to a maximum value $m = M$. In Quiblier (1984), M was chosen to be 12; however when R_y is close to 1, the series converges very slowly. Our data were obtained with $M = 50$; above this value, numerical difficulties such as overflows occurred. In order to give an idea of the numerical precision, let us say that only the three first digits were stable with $M = 30$ for $R_y \leqslant 0.9$; moreover, for various values of ε, $R_z(R_y = 1)$ is equal to ~ 0.9 instead of 1, which illustrates the deterioration of the precision when R_y tends towards 1.

This last difficulty was turned around in the following way. It was supposed that close to 1, R_z can be expanded as

$$R_z = 1 - a_1 \cdot (1 - R_y)^{1/2} + \cdots . \qquad [21]$$

This expansion was suggested by the analytical formula [19]. The constant a_1 depends upon the porosity ε. It was determined by comparison of [21] with the numerical data at $R_y = 0.9$ where the precision is still acceptable. The validity of this expansion was checked by comparing its prediction with the numerical data at $R_y = 0.8$; for instance, for $\varepsilon = 0.1$, one obtains with [21] $R_z(R_y = 0.8) = 0.511$, instead of 0.513 numerically; the fit is thus excellent.

The inverse problem relative to the nonlinear filter consists of the determination of R_y when R_z is known; [15] has thus to be solved. The graphical discussion of this equation is rendered obvious by figure 6. Remember here that the absolute value of a correlation function is always $\leqslant 1$. When $R_z \geqslant R_z(R_y = -1)$, [15] also has a unique solution. Otherwise, this equation does not have any solution. This imposes an extra condition on the experimental function R_z.

R_y was determined as a function of the translation vector $\mathbf{u}$ for the experimental data displayed in figure 5. The results are shown in figure 7 and they can be commented on as follows. The general shape of the correlation functions R_z is conserved; the values which are the most modified are the ones close to 1. It is gratifying to note that for the data analysed here, [15] always has a solution.

A last check was done on R_y. Since they are supposed to be correlation functions, they should also have positive Fourier coefficients. As was done for the experimental R_z, these coefficients were systematically determined for the correlation functions R_y. The same conclusions as before hold; whenever they are negative, the Fourier coefficients are small; if the correlation functions R_y are reconstructed with the negative coefficients set to zero, the difference with the original functions is negligible.

This remark terminates the presentation and discussion of the inverse problem associated with the nonlinear filter. Let us now switch to the linear filter [9].

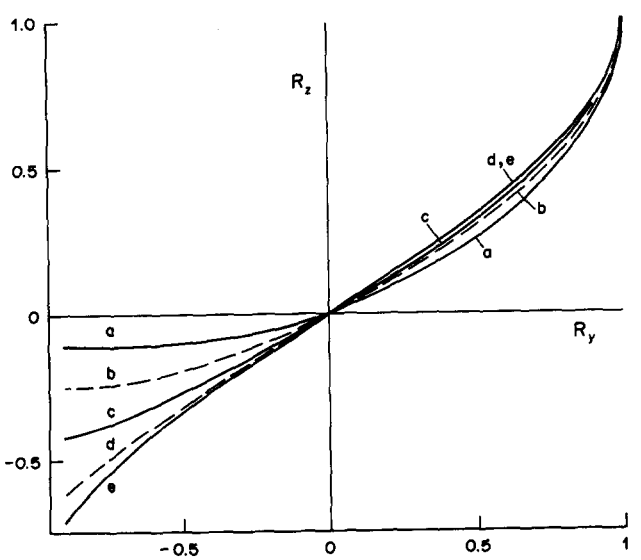

Figure 6. The correlation function R_z as a function of the correlation R_y [15]. Values of the porosity ε are: (a) 0.1; (b) 0.2; (c) 0.3; (d) 0.4; (e) 0.5.

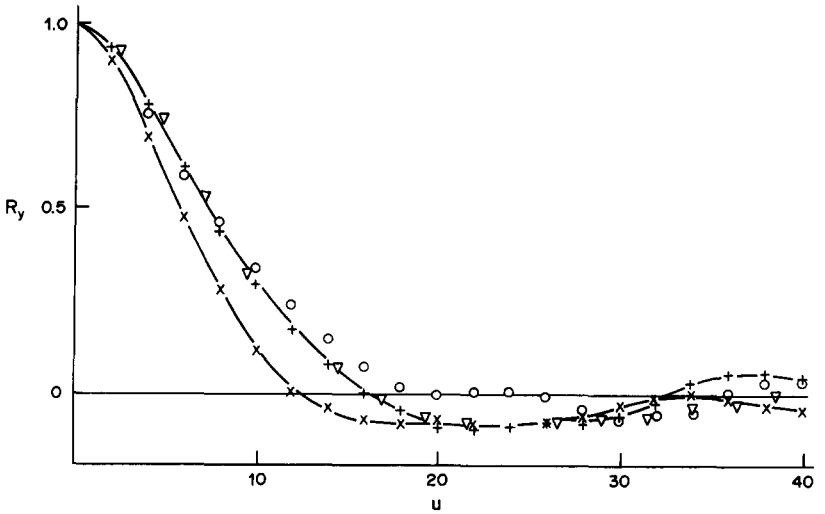

Figure 7. Experimental correlation functions R_y as functions of the translation u. Conditions are the same as in figure 5.

The inverse problem associated with it consists of the determination of the coefficients $\bar{a}$ when $R_y(u)$ is known (cf. [11]).

A few general comments can be made regarding [11]. It is easily seen from examples in one dimension that the solution of [11] is not unique. For instance, for a monodimensional filter with $L_c = 1$, [11] is reduced to the couple of conditions

$$\bar{a}_0^2 + \bar{a}_1^2 = 1, \quad \bar{a}_0 \bar{a}_1 = R_y(1). \tag{22}$$

This system has two positive roots, $\bar{a}_0^2$ if $1 - 4R_y^2$ (Lemaître & Adler 1990) is positive. This condition is equivalent to the nonnegative definite character of the correlation function R_y.

So far we have not been able to generalize this property to any three-dimensional system. This is an important point since the existence of solutions to [11] would be guaranteed by the nonnegative definite character of R_y.

Let us now consider the numerical solution of [11]. Joshi (1974) and Quiblier (1984) solved it directly. This system is quite simple in its structure but it leads to a large number $(L_c + 1)^3$ of unknowns and equations, even for small values of L_c. When the porous media are isotropic, this number can be greatly reduced since the coefficients $\bar{a}_{r,s,t}$ should only be functions of the distance $d = (r^2 + s^2 + t^2)^{1/2}$:

$$\bar{a}_{r,s,t} = \bar{a}(\sqrt{r^2 + s^2 + t^2}). \tag{23}$$

Hence, for isotropic media, one has to determine the function $\bar{a}(d)$ in the $L_c + 1$ points $\bar{a}(d = 0), \ldots, \bar{a}(d = L_c)$; the points located in between are calculated by a given interpolation scheme. The system [11] is reduced to the $L_c + 1$ equations:

$$\sum_{r,s,t \in [0, L_c]} \bar{a}(\sqrt{r^2 + s^2 + t^2}) \cdot \bar{a}(\sqrt{(r+u)^2 + s^2 + t^2}) = R_y(u), \qquad u = 0, \ldots, L_c. \tag{24}$$

This system was solved using a combination of two subroutines of the IMSL Library. Whenever necessary the coefficients $\bar{a}$ are determined by ICSICU which interpolates by cubic splines; a single function is defined as the sum of the squares of the $L_c + 1$ equations [24] and the subroutine ZXMIN calculates a minimum of this function by a quasi-Newton method. It is verified *a posteriori* that this minimum corresponds to a solution of [24].

This combination of subroutines worked quite well; some examples of sets of coefficients $\bar{a}$ are given in table 1, together with the value of the minimum $\mathfrak{M}$ of the function determined by ZXMIN.

Incidentally, it is useless to take into account every point of the correlation R_y. Usually, one point is selected every n points; for instance, $R_y(u = 0)$, $R_y(u = n)$, $R_y(u = 2 \cdot n), \ldots, R_y(u = L_c \cdot n)$ are retained.

Table 1. Coefficients $\bar{a}(d)$ of the linear filter; the images are displayed in figures 1(a – d). Data are for $L_c = 8$ and $n = 4$

	Image			
Coefficients	2A3	GF2	CJ	12A13
$\bar{a}(0)$	−0.1608	0.1141	−0.05350	0.2130
$\bar{a}(1)$	−0.09612	0.1163	0.00163	0.01930
$\bar{a}(2)$	0.04362	0.1981	0.1547	−0.02923
$\bar{a}(3)$	−0.02945	0.09622	0.1641	0.03030
$\bar{a}(4)$	−0.02728	−0.03673	0.04373	0.01642
$\bar{a}(5)$	0.00449	−0.03032	−0.00870	−0.01928
$\bar{a}(6)$	0.05580	−0.01673	−0.00652	0.05862
$\bar{a}(7)$	0.07800	−0.03311	−0.02251	−0.07218
$\bar{a}(8)$	0.02928	−0.3009	−0.01568	−0.05229
$\mathfrak{M}$	$0.15 \cdot 10^{-2}$	$0.35 \cdot 10^{-3}$	$0.59 \cdot 10^{-3}$	$0.52 \cdot 10^{-2}$

Some additional work was done on these coefficients but no general order could be found in the variations of these coefficients. For a given set of data, they appear to be erratic functions of distance. In most cases, negative and positive coefficients are obtained; they all display the same sign only in rare opportunities. When the IMSL subroutine ZXMIN was started from various initial conditions, different solutions were obtained which possessed the same overall precision.

Sets a' and a'' corresponding to the following conditions were also compared for the same correlation R_y. a' was obtained for n and $L_c = 2l_c$, and a'' was obtained for $2n$ and l_c such as the same real distance is explored. However, a' was not found to be the interpolated values of a'', as was expected on intuitive grounds.

Generation of real porous media

Once the coefficients of the linear filter are determined, simulated porous media can be generated at will. It should be emphasized that three "artificial" parameters were introduced in these simulations:

- n the distance between two experimental data;
- L_c the total number of such data;
- N_c the size of the generated cube.

After a general discussion of the average properties of the simulated media, the influence of these parameters will be briefly presented.

Let us first look at the statistical properties of an example of porous medium. Table 2 shows that the agreement between the correlation function of the simulated media and the experimental correlation is pretty good. The influence of the total number of simulated configurations is also clear; one needs to generate at least 5 or 10 such configurations (i.e. $8 \cdot 10^5$ elementary cubes), the agreement is excellent; it is interesting to notice that the average difference between the simulated and the experimental correlation is of the order of magnitude of the error done during the resolution of [24].

Table 2. Statistical properties of simulated porous media. Data are for image GF2, $L_c = 8$, $n = 4$ and $N_c = 20$

$R_c(u)$	δ	$\mathfrak{N} = 1$	$\mathfrak{N} = 5$	$\mathfrak{N} = 10$	$\mathfrak{N} = 20$	$\mathfrak{N} = 100$
1	0.002	1	1	1	1	1
0.465	−0.004	0.501	0.443	0.455	0.457	0.459
0.163	0.003	0.214	0.145	0.165	0.168	0.165
0.006	$-6 \cdot 10^{-3}$	0.064	0.010	0.014	0.013	0.005
−0.038	-10^{-4}	−0.013	−0.032	−0.032	−0.033	−0.042
−0.042	0.002	−0.059	−0.034	−0.041	−0.043	−0.045
−0.045	-10^{-4}	−0.062	−0.046	−0.048	−0.049	−0.047
−0.034	10^{-3}	−0.041	−0.015	−0.040	−0.038	−0.034
−0.011	0.002	−0.006	0.001	−0.016	−0.006	−0.003
$\bar{\varepsilon} = 0.25$		$\bar{\varepsilon} = 0.27$	$\bar{\varepsilon} = 0.25$	$\bar{\varepsilon} = 0.25$	$\bar{\varepsilon} = 0.27$	$\bar{\varepsilon} = 0.25$

The first column recalls the experimental correlation. δ is the residue of each equation of system [24]. Average correlations and porosities $\bar{\varepsilon}$ are given for $\mathfrak{N}$ configurations.

This has been found to be generally the case; whenever the resolution of [24] is not precise, then the average simulated correlation itself is not in good agreement with the experimental correlation it is supposed to fit. For instance, when $n \cdot L_c$ is too small, $R_z(n \cdot L_c)$ may not be sufficiently small; in this situation, as already pointed out in Quiblier (1984), the precision of the solution of [24] is poor and the simulated correlations are also found to be poor.

The influence of the parameters, n, L_c and N_c can now be presented. The choice of this set of parameters is not totally free; the larger N_c, the better; it will be seen in the next section that N_c is limited to 27 presently. L_c should be as large as possible with the constraint that it is at least smaller than N_c.

Before the influence of n is studied, the statistical variations of the generated media are illustrated in figures 8(a–d) for a given set of parameters. The variety of the generated shapes is striking, though similarities between parts (b), (c) and (d) are apparent; part (a) looks different.

The influence of n is illustrated by figures 9(a–d). The images which are presented were deliberately chosen for their average character. The product $n \cdot L_c$ was kept constant in figures 9(a–c), so that the real length of the correlation remains the same from one image to another. Hence, the change of n is simply equivalent to a change of the unit length scale; an arbitrary unit scale is given in figures 9(a–d); for instance, the same real length looks 4 times larger in image (c) than in (a); this is consistent with the visual impression given by these images since image (c) is a plausible magnification of (a); it is also interesting to note that isolated elementary squares are almost absent in image (c). Images (b) and (d) were obtained with $n = 4$ and 3, respectively; the other parameters were identical; no difference is clearly apparent in images (b) and (d).

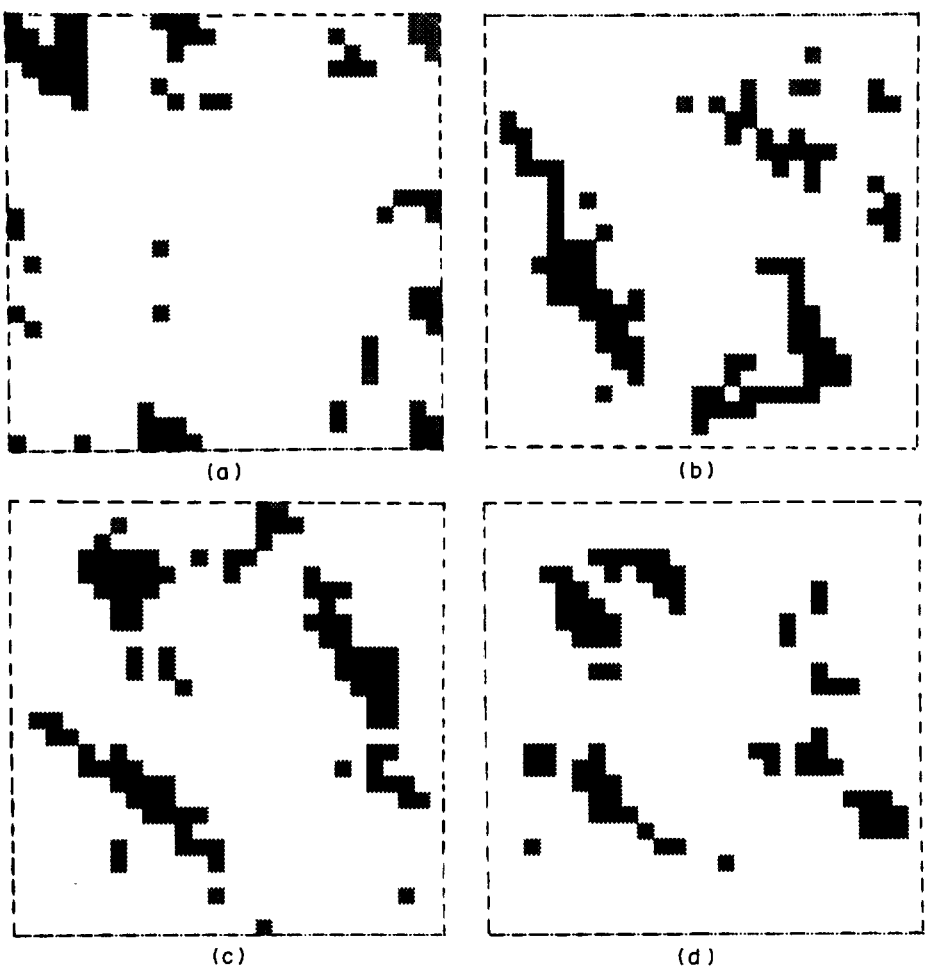

Figure 8. Cross-sections of a sample of simulated porous medium. The pores are black; the solid phase is white; the boundaries of the sample are indicated by the broken lines. This sample has the same characteristics as the image 12A13 ($\varepsilon = 0.11$); $N_c = 27$, $L_c = 8$ and $n = 4$.

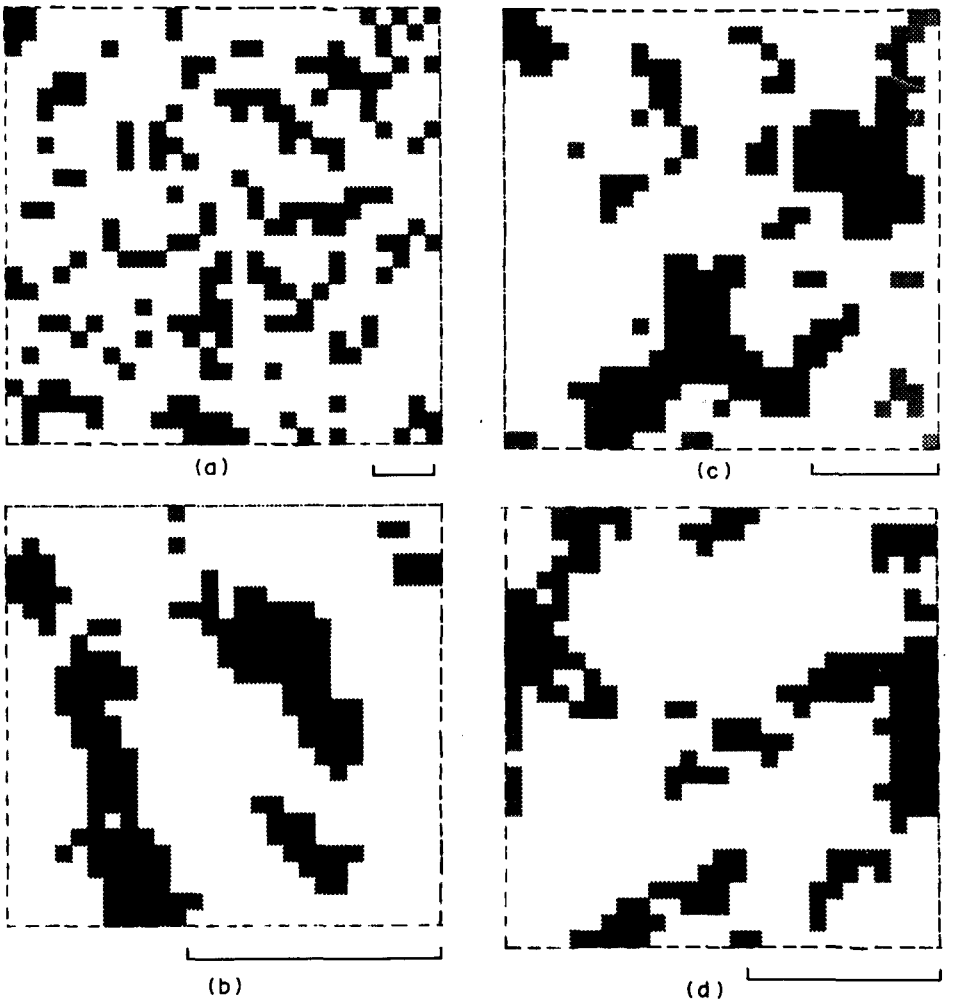

Figure 9. Cross-sections of simulated porous media. Conventions are as given in figure 8. The statistical characteristics are those of the image GF2 ($\varepsilon = 0.25$). $N_c = 27$. Data are for: (a) $L_c = 4$, $n = 8$; (b) $L_c = 8$, $n = 4$; (c) $L_c = 16$, $n = 2$; (d) $L_c = 8$, $n = 3$.

Figure 9(b) can be compared with the real cross-section displayed in figure 1(b). The two figures share a number of features: the random aspect of the cross-section, the connection of a few pores to one another, the existence of several isolated pores.

The influence of porosity on the resulting structure may be more completely examined in figures 10(a–d). The images displayed in figures 1(a–d) have been simulated with the same set of numerical parameters. The results can be commented on in the following way. In figure 10(a) [as is figure 1(a)], the pores are largely connected to one another. As already stated, figure 10(b) [as in figure 9(b)] contains two kinds of pores; some are connected and some isolated. The impression given by figure 10(c) is very different since only four large pores appear; this peculiar feature can be caused by the large experimental correlation R_z (cf. figure 5). Finally, figure 10(d) is mostly composed, as is figure 1, by isolated pores.

Concluding remarks

A few remarks end this section. It can be safely concluded that the simulation process which was devised by Joshi (1974) and Quiblier (1984) works quite well. The porosity and the correlation function are well-reproduced. Moreover, the visual aspect of the simulated cross-sections is not at odds with the aspect of the real ones.

The present work was deliberately restricted to isotropic media; on the numerical side, this restriction only modifies the determination of the coefficients a of the linear filter; the rest of the analysis remains unchanged. It should be emphasized that the additional experimental work

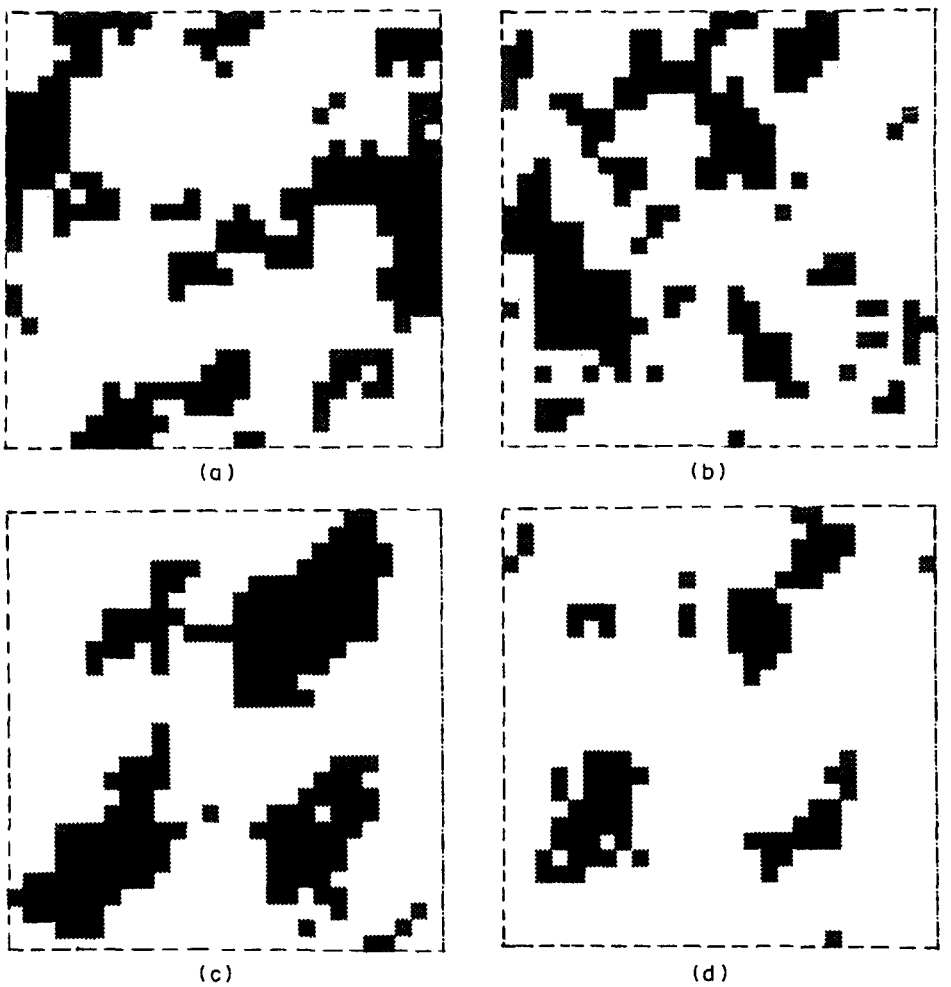

Figure 10. Cross-sections of simulated porous media of various porosities. Conventions are as given in figure 8. The statistical characteristics are those of the images displayed in figures 1(a–d) in the same order. Data are for: $N_c = 27$, $L_c = 8$ and $n = 4$ for (a), (b) and (d); $n = 3$ for (c).

required for the analysis of anisotropic media is considerably larger than the additional numerical effort.

Finally, it will be seen in the next section that the calculation of the flow field imposes extra conditions on the so-called "artificial" parameters N_c, L_c and n.

5. FLOW AND PERMEABILITY

Once finite samples of porous media are generated, the flow field of Newtonian fluids at low Reynolds number can be determined with the program which was first described by Lemaître & Adler (1990).

The flow problem will be briefly recalled here together with a description of the program itself and of its possibilities. In the second paragraph, this program is applied to the porous media which were determined and compared with the experimental data which were presented in section 2.

General

The low Reynolds number flow of an incompressible Newtonian fluid is governed by the usual Stokes equations:

$$\nabla p = \mu \nabla^2 \mathbf{v} \qquad [25a]$$

and

$$\nabla \cdot \mathbf{v} = 0, \qquad [25b]$$

where $\mathbf{v}$, p and μ are the velocity, pressure and viscosity of the fluid, respectively. In general, $\mathbf{v}$ satisfies the conditions

$$\mathbf{v} = 0 \quad \text{on } S, \tag{26a}$$

and

$$\mathbf{v} \text{ is spatially periodic,} \tag{26b}$$

S denotes the surface of the wetted solid inside the unit cell. The volume τ_0 of this cell is equal to $(N_c \cdot a)^3$.

As in section 3, one considers a finite sample of size $N_c \cdot a$ (cf. Lemaître & Adler 1990). This system of equations and the conditions apply locally at each point $\mathbf{R}$ of the interstitial fluid. In addition, it is assumed that either the seepage velocity vector $\mathbf{v}$ is specified, i.e.

$$\mathbf{v} = \frac{1}{\tau_0} \cdot \int_{\partial\tau_0} \mathbf{R}\, \mathrm{ds} \cdot \mathbf{v} = \text{a prescribed constant vector,} \tag{27a}$$

or else that the macroscopic pressure gradient ∇p is specified,

$$\overline{\nabla p} = \text{a prescribed constant vector.} \tag{27b}$$

As is well-known, these two quantities are related by the permeability tensor $\mathbf{K}$ such that

$$\bar{\mathbf{v}} = -\left(\frac{1}{\mu}\right) \mathbf{K} \cdot \nabla p. \tag{28}$$

Here $\mathbf{K}$ is a symmetric tensor that is positive definite. It only depends on the geometry of the system and thus can be simplified when the porous medium possesses geometric symmetries. A good example is given by the regular fractals studied by Lemaître & Adler (1990), which possessed cubic symmetry; hence $\mathbf{K}$ is a spherical tensor, i.e.

$$\mathbf{K} = K\mathbf{I}, \tag{29}$$

where $\mathbf{I}$ is the unit tensor.

The same property holds for the average permeability $\bar{K}$ of the random medium since it is isotropic only in the average.

The numerical method which is used here is the same as that used by Lemaître & Adler (1990). In order to cope with the continuity equation, the so-called artificial compressibility method was applied with a staggered marker-and-cell (MAC) mesh. In essence, the problem is replaced by an unsteady compressible one which is assumed to converge towards the steady incompressible situation of interest.

The number of iterations was minimized by an implicit scheme and the equations were solved successively along each direction; this is the so-called alternating-direction-implicit (ADI) scheme. It will be seen below that the computational times and the necessary memory storage were acceptable. A FORTRAN-77 version of the program is available from the authors upon request. It is quite portable in the sense that it only requires two subroutines of the IMSL Library, namely the generator of independent Gaussian variables GGNML and the interpolator ICSICU.

The mesh spacing Δ is the same in the three directions. It is a fraction $1/N$ of the smallest length which exists in the medium under consideration. Thus, it is given by

$$\Delta = \frac{a}{N}, \tag{30}$$

where N is an integer.

For a given configuration, a numerical integration over one side of the unit cell yields the seepage velocity and K.

Estimation of the permeability may be obtained from the classical Carman equation. Let us omit any distinction between the various components of K: then, K may be expressed as

$$K = \varepsilon \frac{m^2}{k} \tag{31}$$

where m is the hydraulic radius [defined as (free volume/wetted area)] and k is the so-called Kozeny constant. This equation has already been discussed at length by Lemaître & Adler (1990).

It might be the right place at the end of this general presentation to give some computational details since the practical implementation of the routine can sometimes be considered as a problem. All the calculations were performed on a CRAY-XMP.

The maximum memory allowed was 3 megawords in simple precision (i.e. 64 bits). The largest cube which could be calculated with this memory has a size $N_c = 27$ with $N = 2$ (i.e. 8 discretization points/elementary cube).

The time step was usually equal to 0.18 in dimensionless unit. This is surprisingly large and it is surely the key point which rendered the present study feasible. It might be useful to recall that the time step is limited by the occurrence of numerical instabilities; so the larger the time step, the smaller the number of iterations necessary to reach the steady state with an acceptable precision. The program is able to detect numerical instabilities and to start again the calculations for a given configuration with a diminished time step. However, it was empirically found that the time step could not be increased during a given calculation to accelerate convergence: an instability was almost systematically triggered in this case.

Convergence was reached when the flow rate was found the same within $p\%$ across the various sections of the medium. Unless it is mentioned, $p = 1$ in the following. It took sometimes more than 10^4 iterations to obtain the solution.

Let us given an example to be specific. Nineteen porous media corresponding to the image 2A3 were simulated with $N_c = 20$, $N = 2$; the average number of time steps to obtain the convergence was 1450, but it ranged from 580 to 3460. One time step took about 0.36 s on the CRAY; so it took about 9 min in the average to calculate one configuration.

The influence of the discretization parameter N has already been studied by Lemaître & Adler (1990) for the case of random medium derived from site percolation. It was seen that for samples of size $N_c = 10$, its influence was $<8\%$. This error is completely negligible here since larger samples are used and since the statistical fluctuations are $\gg 8\%$. Hence the minimal value $N = 2$ will be systematically utilized in the following.

Results and discussion

The presentation of the results and their discussion is organized as follows. First, a few useful quantities are defined, such as the various possible averages of permeability. Then the large amplitudes of the statistical fluctuations are illustrated by an example; this point is important since it gives an idea of the "precision" of the numerical data. The influence of the artificial geometric parameters n, L_c and N_c is discussed. Once these parameters have been chosen adequately, the permeability is calculated for five samples corresponding to five different porosities and is compared with the experimental data and the predictions of the Carman equation [31]. A general discussion of the possibilities of the present method closes this subsection.

The length of the numerical computations should always be borne in mind throughout the rest of this section; it was simply impossible to explore all the possible combinations of parameters.

The dimensional values of the permeability are given here in Darcy (D) in order to avoid any ambiguity. Permeabilities are known to be equivalent to the square of a length and 1D is very close to 1 μm^2. The dimensional value is derived from the numerical and dimensionless calculations in the following way. During the course of the image analysis, it is easy to determine the length $\alpha(\mu m)$ corresponding to 1 pixel; the experimental correlation is sampled every n pixels. Hence, the size a of the elementary cubes is equal to $n\alpha(\mu m)$. The dimensional permeability K is simply derived from the dimensionless one by multiplying it by $(n\alpha)^2$.

A number of configurations are simulated for a given set of conditions. $\mathfrak{N}$ configurations percolate, i.e. have a nonzero permeability; $\mathfrak{N}_{NP}$ configurations do not percolate. For the sake of completeness, the average permeability K^* of the percolating configurations will be given,

$$K^* = \frac{1}{\mathfrak{N}} \cdot \sum_{i=1}^{\mathfrak{N}} K_i, \qquad [32]$$

as well as the corresponding fluctuations,

$$F = \frac{1}{K^*} \cdot \left[\frac{1}{\mathfrak{N}} \cdot \sum_{i=1}^{\mathfrak{N}} (K_i - K^*)^2 \right]^{1/2}. \qquad [33]$$

However, the average permeability $\bar{K}$ is the average over all the configurations

$$\bar{K} = K^* \cdot \frac{\mathfrak{N}}{\mathfrak{N} + \mathfrak{N}_{NP}}. \quad [34]$$

It is this value which has to be compared with the experimental data.

It is important to appreciate right at the beginning the order of magnitude of the statistical fluctuations. Of course this quantity depends upon the size N_c of the unit cell; on physical grounds, it is expected that the larger the cell, the smaller the fluctuations. This is seen to be qualitatively true in table 3, where some results relative to the sample 2A3 are gathered. The maximum and minimum permeabilities K_{max} and K_{min} of the percolating configurations are also given; these quantities give a precise idea of the range of the fluctuations. Note that the porosity of the configuration corresponding to K_{max} for $N_c = 10$ was equal to 0.66; the final average porosity was 0.36 and, thus, pretty close to the desired value of 0.31.

The influence of the size N_c of the unit cell is not generally important (cf. tables 3 and 4), except when N_c is only slightly larger than L_c. In this case, which is illustrated in table 3 and also in table 4 for the image GF2, K is systematically increased. This effect seems to be mostly due to the generation with periodic boundary conditions of the sample which may bias the long-range correlations for $N_c \sim L_c$. This bias can be totally avoided when $N_c > 2L_c$. When this condition is fulfilled, the data do not appreciably depend upon N_c anymore.

This problem of the size of the unit cell will be addressed again later in slightly different terms.

Large values of N_c, such as 27, were practically quite difficult to study in the present state of the program, especially at low porosities such as 0.14 and 0.10. The program ran during very long times and some of the explored configurations were nonpercolating. Hence, a large amount of computer time was wasted for $N_c = 27$ without any appreciable result.

A good compromise seemed to be obtained for $N_c = 20$. For this value, the statistical fluctuations were not too important and computer time was used efficiently without appreciable loss. Of course, it is hoped that future versions of this program will be more efficient so that larger samples can be studied; they will certainly incorporate a fast exploration and identification of the dead fluid regions and of the nonpercolating configurations.

The influence of the parameter n on the numerical results was briefly analysed. Due to the important computer time which would be required, a systematic analysis was not started; however, its most salient features can be understood.

When n is small, i.e. $n = 2, 4$, its influence on the results is not very important (cf. tables 3 and 4).

However, when large values of the step n were chosen the numerical output was almost non-existent, though the experimental values of the correlation function and of the desired porosity were correctly reproduced by the routine. For instance, the image CJ was utilized with $L_c = 8$, $n = 8$, $N_c = 20$; the first value $R_z(u' = 1)$ of the experimental correlation is about 0.2 and thus quite small. Then six configurations were generated and none was found to be convergent or percolating. At first sight, this failure may appear to be contradictory with the fact that the experimental properties of the porous medium are well-reproduced.

This behaviour can be interpreted as follows. When the first value $R_z(u' = 1)$ of the correlation is small, then two adjacent elementary cubes are almost uncorrelated; one is back to the classical

Table 3. Influence of the parameters N_c and n. The statistical properties correspond to the image 2A3 [cf. figure 1(a)]. Data are for $\varepsilon = 0.31$, $\alpha = 3.8\,\mu$m and $L_c = 8$

N_c	$\mathfrak{N}$	$\mathfrak{N}_{NP}$	K_{min}	K_{max}	F	K^*	$\bar{K}$
			(a) n = 4				
10	100	24	0.25	54	1.5	5.3	4.3
20	19	0	0.86	4	0.33	2.7	2.7
27	5	0	2.1	5.4	0.53	2.8	2.8
			(b) n = 2				
10	100	59	0.16	310	1.8	6.35	4.00
15	96	13	0.097	65	1.4	2.00	1.76
20	18	1	0.03	6.32	1.1	1.49	1.41
25	9	0	0.05	2.54	0.8	0.87	0.87

Table 4. Numerical results for the various samples. Data are for $\alpha = 3.8\,\mu$m (2A3, GF2, 12A13), $\alpha = 4.6$ mm (CJ) and $\alpha = 4.5\,\mu$m (CJDB)

Image	L_c	n	N_c	$\mathfrak{N}$	$\mathfrak{N}_{NP}$	K_{min}	K_{max}	F	K^*	$\bar{K}$	k^*
2A3,	8	4	27	5	0	2.1	5.4	0.53	2.8	2.8	9.3
$\varepsilon = 0.31$	8	4	20	19	0	0.86	4	0.33	2.7	2.7	8.8
GF2,	8	4	27	2	0	0.50	0.85	0.26	0.67	0.67	16
$\varepsilon = 0.25$	8	4	20	11	0	0.31	1.24		0.70	0.70	14
	16	2	20	6	1	0.21	6	1.0	1.85	1.61	11
	8	4	27	1	0	0.26	0.26	0	0.26	0.26	49
CJ,	14	4	27	1	0	0.32	0.32	0	0.32	0.32	36
$\varepsilon = 0.21$	8	4	20	2	0	0.24	0.33	0.16	0.29	0.29	35
	10	3	20	6	3	$0.4 \cdot 10^{-2}$	4	1.3	1.08	0.72	20
CJDB, $\varepsilon = 0.14$	8	4	20	3	4	0.32	0.63	0.27	0.47	0.20	25
12A13,	8	4	20	3	9	0.080	0.50	0.66	0.26	0.065	38
$\varepsilon = 0.11$	8	3	20	5	11	0.029	0.35	0.73	0.15	0.048	52

site percolation which has been studied extensively (Lemaître & Adler 1990). When the porosity is smaller than a critical value $\varepsilon_c \sim 0.3117$, infinite cubic arrays do not percolate. This is exactly what happens here; when the step n is too large, the correlation between two adjacent cubes is too small. Hence, in terms of permeability computations, it is totally useless to try to extend the range of the correlation too much by increasing n beyond reasonable limits.

Conversely, when n is small, adjacent cubes are well-correlated and n does not notably influence the final result—as has already been pointed out.

It may be the right place here to make a specific comment on the quality of the simulation devised by Joshi (1974) and Quiblier (1984). In view of the nonpercolating behaviour at low porosities of porous media devised from site percolation, the verification of the correlation function is essential to obtain percolating media at the relatively low values of the experimental porosities.

All the previous discussions about the so-called artificial parameters n, L_c and N_c can now be summarized.

$a \cdot N_c$ has to be large enough when compared to the correlation length Ω of the medium; this length is distinct from L_c and is necessarily smaller than $\alpha n L_c$ in order to have a good description of the medium; large values of N_c also minimize the statistical fluctuations. However, in the present stage of development of the flow program, too large values of N_c can give rise to a loss in the efficient usage of computer time.

n should be small such that two adjacent elementary cubes are still well-correlated; when the correlation coefficient is of the order of 0.6, good results are generally obtained. Otherwise only nonpercolating configurations are generated.

Finally, $2 \cdot L_c$ should be smaller than N_c because of the periodic boundary conditions.

This study can be summed up by the inequalities

$$1 \ll \frac{\Omega}{\alpha n} < L_c < \frac{N_c}{2}. \qquad [35]$$

Of course the stronger these inequalities are, the better, but this may prove to be unfeasible, as noted before. An acceptable compromise between these constraints was empirically found to be (for the length scales α which are used here):

$$N_c = 20, \quad L_c = 8, \quad n = 4. \qquad [36]$$

Most of the definitive calculations were obtained with this set of values.

All the numerical results are collated in table 4, with the minimum of overlap with table 3. Around the values [36] of the parameters, there is no dramatic shift in the permeability. It is important to remember in the remainder of this section that the number of computer configurations is too small; the average permeabilities which are given should only be considered as orders of magnitude rather than precise values.

The values of $\bar{K}$ for (GF2, $L_c = 16$, $n = 2$, $N_c = 20$) and (CJ, $L_c = 10$, $n = 3$, $N_c = 20$) are strongly biased by exceptional configurations. It should be observed that, again, for the first of these two configurations, $\bar{K}$ is slightly higher when $L_c \sim N_c$; the same observation can be made for table 3.

Finally, the average permeability $\bar{K}$ obtained for the parameters [36] was compared with the experimental values in figure 2; it is important to note that this comparison does not involve any hidden adjusted parameter and that every quantity is measured or calculated. The calculated permeability differs by, at most, a factor 5 from the measured one. However, the general shape of the experimental curve is predicted in quite an accurate way as if a systematic "error" was incorporated in the measurement of the unit scale.

It is also seen in table 4 that the Carman equation is not well-verified. k^* denotes the average of the Kozeny constant for each percolating configuration:

$$k^* = \frac{1}{\mathfrak{N}} \cdot \sum_{i=1}^{\mathfrak{N}} \frac{\varepsilon_{a,i}^3}{S_i'^2 K_i}, \qquad [37]$$

where S_i' is the measured wetted area per unit volume and $\varepsilon_{a,i}$ is the actual porosity of the simulated configuration i. Even in the best case, k^* is about twice the standard value of 5. This is, of course, related to the fact that the predicted permeability is too low when compared to the experimental values.

This paper can be ended by putting forward some tentative ideas about this discrepancy between the numerical and experimental permeabilities. Three facts may cause it:

(1) The first and simplest idea is to try to work on larger samples in order to better use, with small n, the experimental correlation and to minimize the statistical fluctuations. This will be deferred to future versions of the program.

(2) There exists a basic difference between the numerical model and the real experiment. In the former, a single elementary cube can block the whole flow without disturbing the average statistical properties of the sample; this situation is never exactly realized in experiments where the fluid can filter through even very small constrictions; moreover, permeability is measured on large samples (which would correspond roughly to $N_c = 170$, $n = 4$) where such blocking effects are minimized. Such large values of N_c are not totally out of reach with the present developments in computer technology. Finite-size effects could also be minimized with large N_c.

(3) The last reason is more subtle and may be caused by the simulation process itself. Only two statistical properties of the real media are fitted in the present model and this may not be sufficient to approximate their geometry with acceptable precision for a transport quantity such as permeability which is very sensitive to connectivity.

REFERENCES

ADLER, P. M. 1989 Flow in porous media. In *The Fractal Approach to Heterogeneous Chemistry* (Edited by AVNIR, D.). Wiley, New York.

ADLER, R. J. 1981 *The Geometry of Random Fields*. Wiley, New York.

BOURBIÉ, T., COUSSY, O. & ZINSZNER, B. 1986 *Acoustique des Milieux Poreux*. Technip, Paris.

GRADSHTEYN, I. S. & RYSHIK, I. M. 1965 *Table of Integrals. Series and Products*. Academic Press, New York.

HENRIETTE, A., JACQUIN, C. G. & ADLER, P. M. 1989 The effective permeability of heterogeneous porous media. *Physicochem. Hydrodynam.* **11**, 63.

JACQUIN, C. G. 1964 Corrélation entre la perméabilité et les caractéristiques géométriques du grès de Fontainebleau. *Revue Inst. fr. Pétrole* **19**, 921–937.

JOSHI, M. 1974 Ph.D. Thesis, Univ. of Kansas, Lawrence, Kans.

LEMAÎTRE, R. & ADLER, P. M. 1990 Fractal porous media, IV. Three-dimensional Stokes flow through random media and regular fractals. *Transp. Porous Media.* Accepted for publication.

QUIBLIER, J. A. 1984 A new three-dimensional modeling technique for studying porous media. *J. Colloid Interface Sci.* **98,** 84–102.

ZINSZNER, B. & MEYNOT, C. 1982 Visualisation des propriétés capillaires des roches réservoirs. *Revue Inst. fr. Pétrole* **39,** 337–361.